ADVANCES IN GEODESY AND GEOINFORMATION
(formerly GEODESY AND CARTOGRAPHY)
Vol. 74, no. 1, article no. e66, 2025

https://doi.org/10.24425/agg.2025.154150

Original paper

Part of Topical collection:
"Advancements in Applied Geoinformatics"

Delineation of debris-covered glaciers with multi-temporal UAV images (Gössnitzkees, Schober Group /Austria)

Harald Zandler[1]*, Wolfgang Sulzer[1], Viktor Kaufmann[2]

[1]University of Graz, Graz, Austria
e-mail: harald.zandler@uni-graz.at; ORCID: http://orcid.org/0000-0001-5505-2455
e-mail: wolfgang.sulzer@uni-graz.at; ORCID: http://orcid.org/0000-0001-6040-2405

[2]Graz University of Technology, Graz, Austria
e-mail: viktor.kaufmann@tugraz.at; ORCID: http://orcid.org/0000-0003-2074-1992

*Corresponding author: Harald Zandler, e-mail: harald.zandler@uni-graz.at

Received: 2024-10-18 / Accepted: 2025-03-31

Abstract: The relative share of debris-covered glaciers strongly increased in recent decades due to climate change and amplified rock production, but despite their relevance as climate indicators, accurate demarcation of respective glaciers is challenging. Remote sensing is an important tool for glacier mapping, but most existing studies apply medium resolution sensors, which are not suitable for small, rock covered glaciers, or use semi-automatic approaches. We present a simple methodology to automatically derive debris-covered glacier areas by using multitemporal, high resolution UAV images. Thereby, standard products, such as elevation differences calculated from digital surface models and displacement rasters, combined with statistical or error thresholds, provide the basis to automatically delineate glacier areas. The comparison of the automatically derived debris-covered glacier area to the geodetically determined glacier snout showed lowest errors for the elevation-based method using yearly data (total error of 0.32 m or 8.6% of the yearly glacier retreat) and higher errors for four-year intervals (0.97 m, 34% of the yearly glacier retreat) or displacement-based methods (0.51 m, 13.6% of the yearly glacier retreat with yearly epochs). Visual evaluation also showed strong errors of the displacement-based method with many areas wrongly identified as debris-covered glacier area. We conclude that the elevation-based method allows for accurate delineation of debris-covered glaciers and pro-glacial areas, providing increased standardization of glacier monitoring using remote sensing.

Keywords: UAV, remote sensing, glacier boundary, Gössnitzkees, debris-covered glacier

1. Introduction

In recent decades, debris cover of glaciers outside the polar regions steadily grew, showing strong areal increases of 10% to 20% over about 20 to 30 years (Kellerer-Pirklbauer, 2008; Azzoni et al., 2018; Mayr and Hagg, 2019; Shukla and Garg, 2019; Fleischer et al., 2021; Tielidze et al., 2024; Zhou et al., 2024). This strong increase and the significant share of debris covered glaciers in mountain regions, whereby the relative mean debris coverage of glaciers was around 23% in the Eastern Alps in 2015 (Fleischer et al., 2021), makes mapping of such glaciers a prerequisite to correctly assess the state of the alpine cryosphere and to monitor connected issues, such as freshwater supply or natural hazards. However, despite the relevance of accurate glacier mapping to study these important climate indicators (Sahu and Gupta, 2018), delineation of debris-covered glaciers is still connected to major research challenges (Xie et al., 2020; Yang et al., 2024). Remote sensing is currently the main tool to derive glacier boundaries and several approaches exist for glacier mapping (Khan et al., 2020). However, climate change and increased rock production lead to excessive debris coverage of many existing glaciers. This makes clear demarcation of these glaciers difficult, as their surfaces are characterized by strong optical similarity to proglacial areas.

Existing approaches to delineate debris-covered glaciers mainly use medium resolution satellite data, including spectral bands, indices, Synthetic Aperture Radar (SAR) and Digital Surface Model (DSM) based topography indicators (Paul et al., 2004; Bolch et al., 2007; Mölg et al., 2018), but most of respective approaches are only suitable for large areas and not small glaciers (Sahu and Gupta, 2018). Thereby, machine learning is a main tool for satellite-based glacier classification (Khan et al., 2020), but delineation of debris-covered areas often also requires manual efforts for correct mapping (Barr et al., 2018). Object based image analysis (OBIA) methods showed some improvements for automatic mapping compared to pixel based methods on larger glaciers (Robson et al., 2016). Additionally, Foster et al. (2012) introduced a method for estimating supraglacial debris thickness from thermal band remote-sensing data.

Recently, the advance of deep learning and convolutional neural networks led to improvements in delimiting debris-covered glaciers (Xie et al., 2020; Yang et al., 2024), and combining OBIA and deep learning showed good performance with satellite based approaches (Thomas et al., 2023). Mentioned studies focus on larger glaciers, often characterized by distinctive morphological features, and exclude very small glaciers or glaciers without clearly developed glacier tongues, which are now typical for many remaining glaciers in the alps (Huss and Fischer, 2016). Studying minor glaciers or glaciers with smaller changes requires higher resolution datasets, and methods based on data obtained by unoccupied aerial vehicles (UAVs) show promising results for debris-covered glaciers (Fugazza et al., 2015; Azzoni et al., 2018). Therefore, UAVs became increasingly popular for studying glacial changes in recent years (Piermattei et al., 2015; Sledz et al., 2021). Existing UAV methods mostly used semi-automatic methods or approaches that require intensive manual mapping to classify debris-covered glaciers. Fully automatic approaches to demarcate debris-covered glaciers from UAV images are scarce. Therefore, the presented approach aims to improve mapping of debris-covered glaciers by examining

possibilities of automated demarcation with bitemporal UAV flights by analyzing height changes and displacement vectors at the glacier margins. A main focus is on testing simple standardized approaches without additional input of field data. A comparison of different automatic methods for defining the glacial margin intends to contribute to better understanding of glaciers as central climate indicators.

2. Methods

2.1. Study area and survey history

The research covers the terminus of the Gössnitzkess that is located in the Schober group of the Hohe Tauern mountain range in the district of Heiligenblut, Carinthia, in Austria (Fig. 1), at around 12.75° to 12.77° Longitude East and 46.96° to 46.97° Latitude North with a total area of 15.24 ha. Due to the high altitude, the area is a high mountain ecosystem with occasional scree or riparian vegetation. Thereby, "kees" is the local term for glacier. The glacier is a typical cirque glacier and is fed primarily by avalanches from the surrounding couloirs. There is no larger accumulation area for snow and ice. The strong debris cover is characteristic of the glacier and of the entire Schober group (Lang and Lieb, 1993). This study focusses on the period 2018–2023. However, the Gössnitzkees has been monitored annually using simple edge measurements as part of the glacier measurement service of the Austrian Alpine Club since 1982. In addition, measurements of longitudinal glacier profiles, terrestrial photos and aerial photo evaluations in 1954, 1983, 1997, 2006

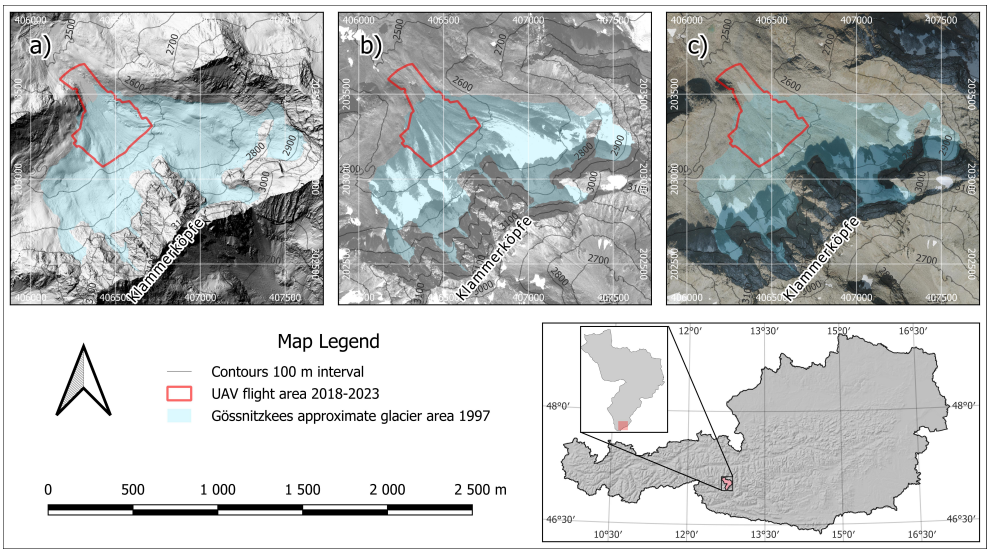

Fig. 1. Overview of the research area showing the general location of the site in the district of Heiligenblut (lower part, EPSG 3416) and (a) the ALS based DSM of the year 2012 (Land Kärnten 2012), (b) the orthophoto of the year 1997 (Land Kärnten 1997) and (c) the orthophoto of 2021 (Land Kärnten 2021), all in EPSG 31258. Graphical scale refers to (a), (b) and (c)

and 2012 were conducted (Kaufmann and Ladstädter, 2008a; 2008b; Kaufmann and Sulzer, 2019). The change in position of the glacier tongue is well documented by annual surveys (trilateration, 1982–2002; tachymetry, spanning 1996–2013 and since 2014, Real-Time Kinematic Global Navigation Satellite Systems (RTK-GNSS) measurements).

Using Gössnitzkees as an example, Kaufmann and Sulzer (2019) recommend the following procedure for long-term monitoring of small glaciers (in Austria): (1) Overall evaluation, approximately every three years, from aerial photographs of the Austrian surveying service (BEV) and annual measurement of the glacier face and at least one longitudinal profile with RTK-GNSS and, if necessary, (3) additional evaluations from UAV flights or terrestrial photogrammetric images (optionally terrestrial laser-scanning) with (4) simultaneous integration of existing airborne laser-scanning (ALS) data. During

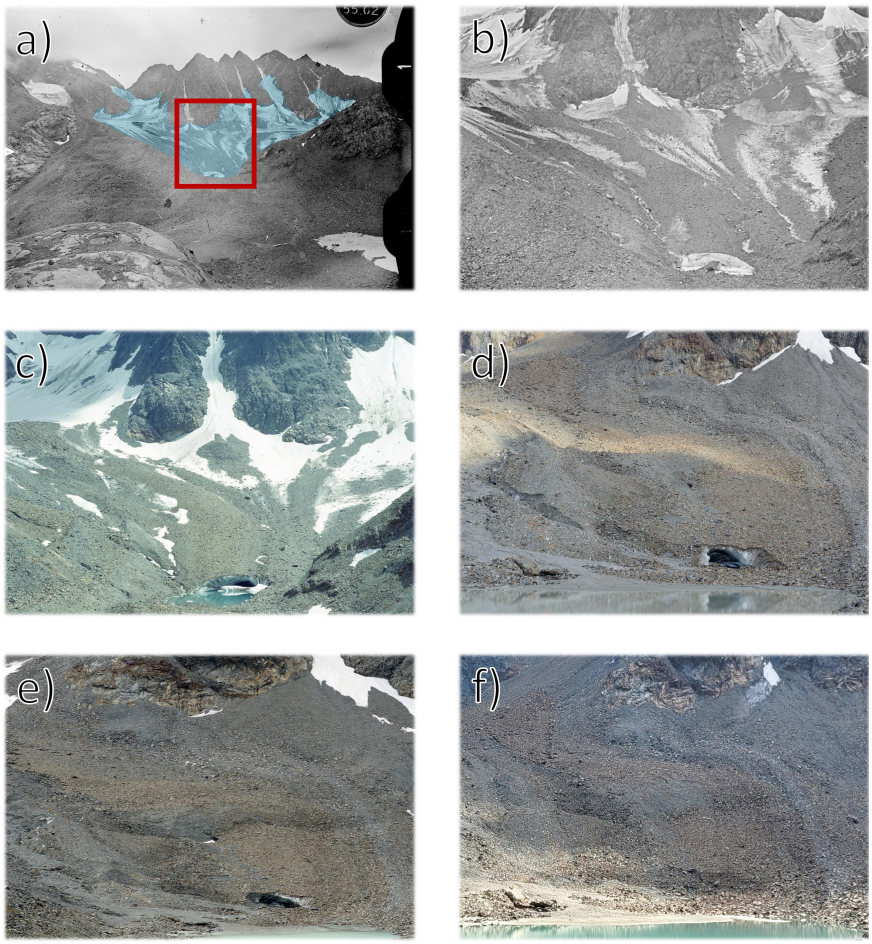

Fig. 2. Photo documentation of the glacier development with (a) an overview during the year 1988 showing the glacier outline and the approximate location of detailed images of the glacier snout in (b) 1988, (c) 1997, (d) 2018, (e) 2019 and (f) 2023

the measurements in the trilateration period, the ice edge in the debris-covered area of the glacier tongue had to be dug by hand to achieve a precise demarcation of the glacier, as visual demarcation from surface features was not possible. Therefore, the detection of the glacier tongue remains challenging with the mentioned traditional methods due to the debris cover, the surrounding debris with a similar grain size and the lack of "typical" glacier morphology with distinctive convex features.

In addition to measurements, a photo documentation of the glacier exists. A comparison of the developments since 1988 clearly shows the challenges connected to glacier demarcation during recent years, as the definition of the transition zone of the glacier to the paraglacial zone is difficult (Fig. 2).

2.2. Geodetic measurements

Ground truth and validation data to accurately determine the glacier snout and evaluate the resulting UAV datasets was collected during several geodetic measurement campaigns in 2018, 2019 and 2023 using RTK-GNSS measurements. Geodetic measurements from 1996 until 2023 can also be downloaded from Kaufmann (2024). Thereby, a local geodetic network of fixed points was established using cadastre points on surrounding mountain tops with classical triangulation. Yearly geodetic measurements, whereby RTK-GNSS measurements were based on the local geodetic network, covered the glacial snout, whereby measurements were based on accessibility, receiver connection and the recording of the main vertices of the snout, and also included transects along the longitudinal axis of the glacier (Fig. 3). The main validation product for the final automatic demarcation was the geodetically derived glacier snout (Fig. 3a), whereby a line was created by connecting the measurement points. To create equally spaced evaluation points, ten points per meter were regularly placed along respective polyline. These points served as the ground truth reference and the minimum distance to the automatically derived glacier area was used as the main performance measure of the approach. Error measures were calculated using the software R (R Core Team, 2024), version 4.3.3., in particular the packages sf (Pebesma, 2018; Pebesma and Bivand, 2023) and terra (Hijmans et al., 2024).

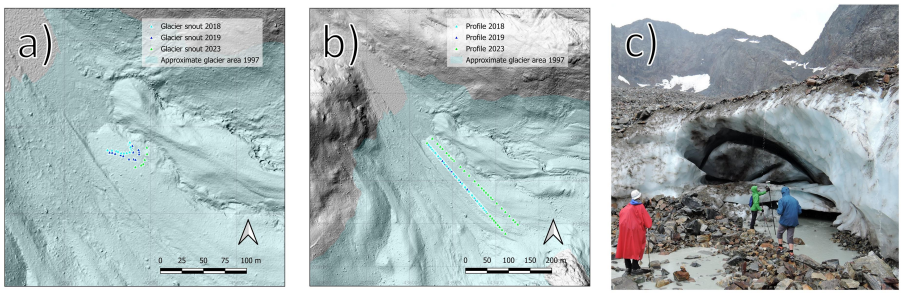

Fig. 3. (a) Geodetic measurement points of the glacier snout, (b) along longitudinal transects covering the glacier, and (c) the photo documentation of the measurement process by V. Kaufmann. The DSM of the background maps is from 2012 (Land Kärnten 2012)

2.3. UAV surveys

UAV surveys were conducted in the years 2018, 2019 and 2023, referred to as epochs herein. Survey years were differently spaced to test different monitoring strategies (one year vs. several years) as outlined in Kaufmann and Sulzer (2019). Due to the remote location of the glacier, a relatively lightweight DJI Phantom 4 with a 12-megapixel camera was deployed for collecting images at a flight height of approximately 70 m, which resulted in a ground sampling distance of around 4 cm. Respective UAV does not have RTK-GNSS capabilities and hence, black-yellow disks with a diameter of 35 cm were used for accurate georeferencing. For error evaluation, one third to half of these points served as reference (Table 1). These points, referred to as check points, were not used in the bundle block adjustment but used for calculating independent errors only. Points used in the bundle block adjustment are referred to as ground control points (GCPs). Placement of GCPs and check point followed standard criteria for structure from motion approaches (Westoby et al., 2012). The changing surface of the glacier prevented the placement of targets at identical positions between the years, leading to differences in GCPs between the surveys. Recent research also showed that check point errors do not decrease with additional GCPs after a certain threshold is reached and errors saturated at about eight GCPs in a much larger research area (Wecht, 2021), which makes the placement of larger numbers of GCPs not feasible. Furthermore, placement was connected to practical constraints, such as the weather situation during the survey, which may limit the temporal resources for GCP placement. Accordingly, the number of GCPs between the years varied but always contained a certain minimum number according to recommendations in literature. Orthoimages and DSMs were calculated using Agisoft Metashape Version 2.1.2 for the years 2018, 2019 and 2023. Final coregistered rasters were resampled to a resolution of 4 cm. Furthermore, geodetic measurements along the transects were used for independent evaluation of the UAV-DSM errors on supraglacial rocks. Thereby, the mean absolute error (MAE), the root mean squared error (RMSE) and the bias were calculated. Formulas for respective performance measures are outlined in Zandler et al., (2019).

Table 1. Ground control points and check points used for the UAV surveys

Year	GCPs	Check points
2018	11	7
2019	18	5
2023	6	6

2.4. DSM differences and displacement calculations

For calculating DSM differences, the DSM raster of the preceding epoch was subtracted from the DSM of the temporally following epoch. The difference raster was subsequently used for automatically deriving the glacier area.

For calculating displacement, two different methods were tested, as suggested in existing research for medium velocities (Jawak et al., 2018; Mueting and Bookhagen, 2023). The first algorithm was IMCORR (Fahnestock et al., 1992; Scambos et al., 1992; Bremer, 2012), which is implemented in SAGA GIS 9.3.1 (Conrad et al., 2015) and uses normalized cross-covariance of fast fourier-transformed images. Thereby, small subsets of the images, called chips or windows, are used and compared between the images. If a match is found, displacement values can be derived. Furthermore, the comparable geoCosiCorr3D method was selected (Aati et al., 2022), which is a newer improvement of the COSI-Corr algorithm (Leprince et al., 2007), as this method is recommended for this purpose in a comparison study (Jawak et al., 2018). The geoCosiCorr3D algorithm uses a multi-scale sliding window, with the first window trying to maximize the correlation, while subsequent smaller sizes enable better displacement estimations (Aati et al., 2022). Similar to IMCORR, it also uses a frequency correlation. Window sizes of 64×64 pixels (256 cm) and 256×256 pixels (1024 cm) and step sizes of 32 cm and 100 cm were tested. Both methods use single band rasters as input. Therefore, the first principal component of the three RGB-bands of the orthophoto was calculated and used in all algorithms. In case of IMCORR, which results in point data and not a displacement raster, an inverse distance interpolation was performed to create final displacement rasters with a side length of 32 cm.

2.5. Attempt of an automatic derivation of the glacier area

The presented method intends to use easy but effective methods and principles to derive glacier areas. Thereby, DSM difference and the displacement rasters serve as main products to automatically derive glacier areas. Kernel density estimation of all raster values was used to create density curves. Respective curves were the basis for threshold derivation for the elevation difference-based approach.

For the delineation approach using elevation differences, the leading principle was that glacier areas show strong surface changes due to ice melt. In contrast, paraglacial areas, with the exception of large gravitational mass movements, are characterized by small surface changes. However, these minor changes around zero are expected to be much more common (high density, i.e. the main peak of the density curve) compared to strong glacial changes (i.e. a secondary peak of the density curve). Therefore, an automatic peak and valley detection algorithm using the R-package *pracma* (Borchers, 2023) was applied to find the valley before the main peak around zero. Respective minimum value before the ascend to the data peak was used as a threshold to define glacier areas of the initial year of the DSM-difference pair, i.e. all values with change larger than the threshold were considered as glacier areas of the earlier epoch.

The other theoretical concept and approach was that glacial flow is a main characteristic of active glaciers in comparison to rocks and dead ice bodies that ceased to flow (Kellerer-Pirklbauer et al., 2021). Therefore, all areas that show displacement beyond an error value, which is defined by the accuracy assessment of the UAV survey, may be considered as glacier area. Respective approach could potentially be extended using the density curve to exclude very large, unlikely displacements. Finally, small isolated patches of under 100 m^2 were removed from the glacier area rasters using the R-package *smoothr* (Strimas-Mackey, 2023).

3. Results

3.1. UAV surveys

The internal evaluation of the aerial triangulation using independent check points showed total three-dimensional errors of about 3.2 cm to 5.5 cm (Table 2). Highest errors were not constant between the years and were found in the X, Y or Z domain. Horizontal errors were around 3 cm to 5 cm per epoch. The cumulated horizontal error of two epochs, which amounts to 8–9 cm, serves as an orientation for building a threshold for the automatic glacier demarcation using the displacement data. Therefore, to use a conservative threshold for the displacement-based method without additionally field mapping, the maximum summed error of two epochs (i.e., 9 cm) was used as the threshold for the automatic glacier demarcation using the displacement data.

Table 2. Error measures of the UAV surveys using independent check points (in cm)

Year	n	X	Y	Z	Total XY	Total XYZ
2018	7	3.09	2.03	3.59	3.70	5.15
2019	5	3.00	3.84	2.66	4.87	5.55
2023	6	2.22	1.86	1.30	2.90	3.17

The additional evaluation of altitudes on supraglacial rock surfaces along the transects showed higher errors with maxima around ten centimeters (Table 3). This error may be used for an alternative threshold for a glacier delineation using DSM differences, but due to the requirement of additional field data, this method cannot be considered automatic.

The visual assessment shows that higher errors were calculated at the lower and upper ends of the transects in 2018 and 2019, whereas the 2023 survey shows relatively uniform error magnitudes along the elevation transects (Fig. 4).

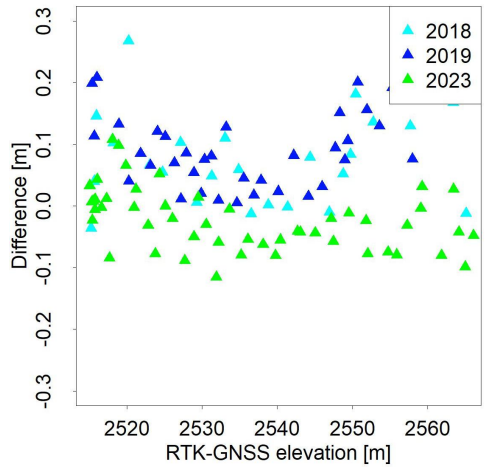

Fig. 4. Differences between the RTK-GNSS survey and UAV derived DSM altitudes along the elevation transects

Table 3. Elevation error measures on rock surfaces along the transect points on the glacier in meters

Year	n	MAE	RMSE	Bias
2018	25	0.08	0.11	0.08
2019	35	0.09	0.10	0.09
2023	65	0.05	0.06	-0.02

3.2. DSM differences

The differences of the one-year period 2018 to 2019 showed a decline of about 1 m to 1.5 m in height on the glacier, 2 m at the western part of the glacier and up to 4 m decrease along the tongue and glacier rim (Fig. 5).

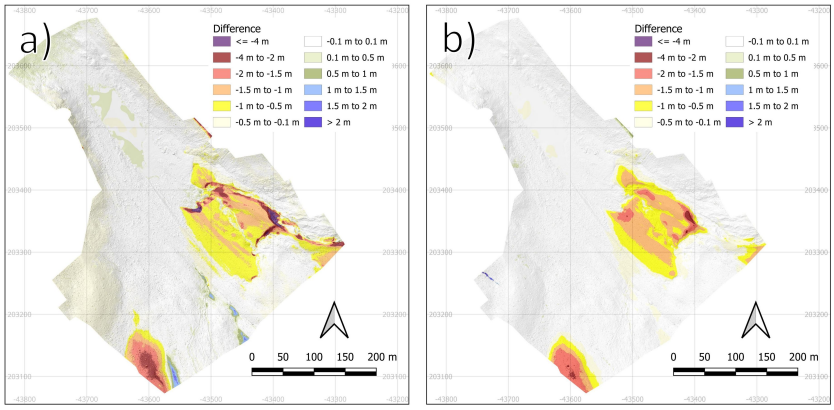

Fig. 5. Annual DSM differences between the epochs (a) 2018–2019 and (b) 2019–2023

The differences between the four-year period 2019 to 2023 showed considerably higher absolute values, but annual differences were much lower at the margins and partly higher in some interior areas. Increases were rarely found and were located in small depressions. Respective areas were characterized by remaining snow fields during the 2019 survey.

3.3. Surface velocities

Results of IMCORR and geoCosiCorr3D were mostly identical. Both results showed glacial movements around 20 cm to 50 cm between the period 2018 to 2019 (Fig. 6). Furthermore, both methods showed a noticeable number of artifacts, particularly on water surfaces but also in some other areas. The epoch from 2019 to 2023 resulted in stronger artifacts and inferior visual results due to increased data decorrelation. This issue could be minimized by analyzing uncorrelated individual measurements (e.g. using manually mapped displacement vectors), which are then used for a filtering approach that worked well on rock glaciers in existing research (Kaufmann et al., 2019). However, such an approach would divert from the aim of an automatic and simple approach and was therefore not applied in the presented manuscript.

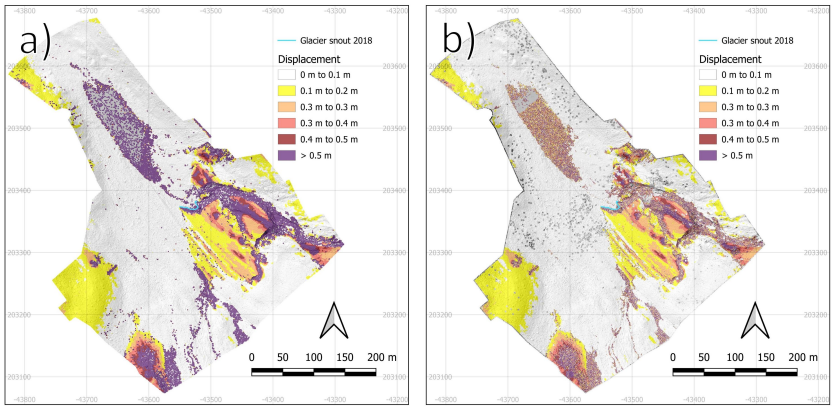

Fig. 6. Displacement 2018–2019 calculated with (a) IMCORR and (b) geoCosiCorr3D

3.4. Automatic glacier delineation

3.4.1. DSM difference method

Density plots for the yearly epochs from 2018–2019 showed a clear bimodal distribution with a higher peak for differences around zero and another peak with stronger negative differences. Automatic peak-valley detection using regular rising and falling pattern of the curve resulted in a threshold for glaciers if the decline is more than 0.61 m (Fig. 7). The comparison of the epochs 2019–2023 shows a similar peak around zero, but the elevation changes were more equally distributed and the second data peak was comparatively flat. The automatically derived threshold value was –1.41 m for this period, meaning that all areas with a decline more than 1.41 m over the four year period were classified as glaciers.

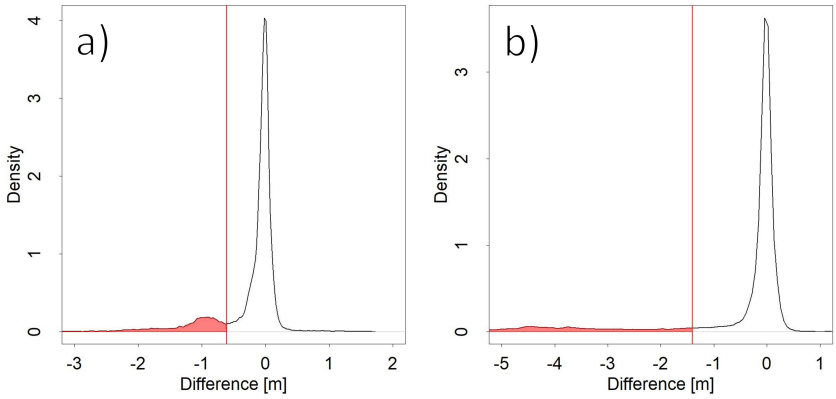

Fig. 7. Kernel density plots of DSM differences and automatically derived glacier values below the threshold (red) for the epochs (a) 2018–2019 and (b) 2019–2023

Visually, respective thresholds showed good agreement with the geodetically derived glacier snout (Fig. 8). Errors amounted to a mean difference of 0.32 m in 2018 and 0.97 m in 2019 between the geodetically derived glacier snout and the automatically derived glacier area.

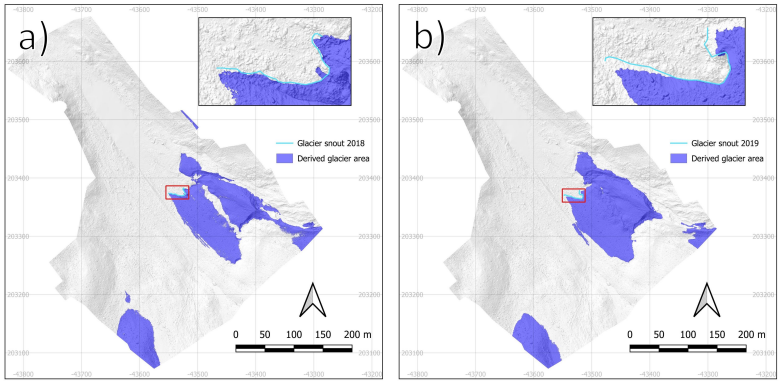

Fig. 8. Automatically derived glacier area using DSM differences compared to (a) the geodetically measured glacier snout in 2018 using the epochs 2018–2019 and (b) the geodetically derived glacier snout in 2019 using the epochs 2019–2023

If compared to the total retreat of the glacier snout between 2017 and 2018 of 3.74 m, the error amounts to 8.6% of the total change in the reference period. Regarding the comparison to the total retreat of 2.85 m from 2018 to 2019, the relative error of the 2019 result is 34.0%.

3.4.2. Displacement based method

The automatic glacier area demarcation using displacement data resulted in a relatively large derived glacier area, but showed a close proximity to the geodetically derived glacier snout (Fig. 9). Calculated errors using epochs 2018–2019 amounted to 0.51 m compared

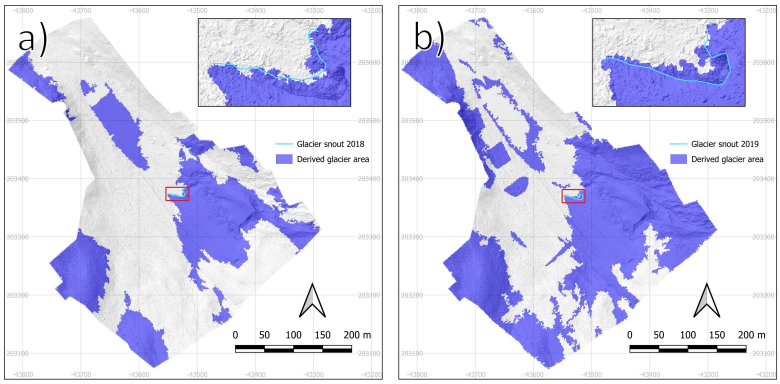

Fig. 9. Automatically derived glacier area using surface displacement results compared to (a) the geodetically measured glacier snout in 2018 using the epochs 2018–2019 and (b) the geodetically derived glacier snout in 2019 using the epochs 2019–2023

to the measured glacier snout in 2018 and 1.89 m compared to the glacier snout 2019 if using the epochs 2019–2023. Respective errors are 13.6% of the total change 2017-2018 and 66.3% of the total change 2018–2019.

4. Discussion

This is the first study that automatically delineates the terminus of small, debris-covered glaciers using standard products of UAV surveys and simple demarcation metrics. Results of annual epochs and with the elevation-difference methods showed low errors and accuracies similar to other, non-automatic approaches (Azzoni et al., 2018), although comparisons to other research is difficult due to methodological dissimilarities. The utilization of longer periods showed comparably high errors and the results indicate that annual periods are an important prerequisite for accurate automatic delineation of debris-covered glaciers with the presented method, which is in line with other studies recommending annual or higher temporal resolutions for glacier monitoring (Immerzeel et al., 2014; Ewertowski et al., 2019; Avian et al., 2020).

The DSM difference-based approach showed good results in the presented setting and research area, but main limitations have to be considered. Gravitational mass movements of greater magnitude would obviously lead to false glacier detection with this approach, whereas smaller changes, such as sediment reworking or small fluvial changes, which are typical for glacial areas (Di Rita et al., 2020), should be excluded by the selected algorithm. False detections caused by larger gravitational mass movements can be limited by confining the automatic algorithms to existing glacier outlines or glacier inventories (Patzelt, 1980; Lambrecht and Kuhn, 2007). Furthermore, another option would be the connection to glacier velocities, e.g., an additional rule set considering only areas beyond the DSM threshold and also with regular surface movements. The visual evaluation also showed that the automatic threshold may be partly too conservative, which is illustrated by areas within the glacier body that were not classified as a glacier in 2018, but were considered as glacier area in the year 2019.

In contrast to the presented automatic threshold derivation method, error-based approaches, i.e. using the independent GNSS measured elevation transects, would be another more traditional method to derive thresholds for glacier demarcation. Using the elevation error of the validation transects as a threshold, which resulted in an error/threshold of about 10 cm in this study, would lead to lower errors if compared to the glacier snout (22 cm for the 2018 glacier margin and 28 cm for the 2019 glacier margin) compared to the automatic approach, but would lead to substantially increased glacier artefacts in areas of small changes due to other processes (sediment reworking, snow, erosion) and would be dependent on additional field data, deviating from the aim to explore an automatic delineation approach. However, the error threshold approach also shows that it may be more suitable for more than one-year intervals, as the 2019–2023 error is only slightly larger than the yearly interval.

Accurate, UAV derived products are the main foundation for deriving glacier areas. The error assessment of the UAV survey showed low errors below 6 cm in total on the target check points, which is relatively low compared to other studies using non RTK UAVs (Piermattei et al., 2015). Higher errors were detected along the elevation profiles, whereby

the main explanation is that check points use targets with a 35 cm diameter, i.e. a flat surface, whereas the elevation profiles were measured directly on the rock surface with strong microtopography (e.g. cracks between rocks), which can lead to strong elevation differences even with very small horizontal offsets. However, these errors, which were also below 10 cm, may be considered sufficient for delineating debris-covered glaciers and comparable to other state of the art methods for topographic analysis (Yurtseven, 2019).

The displacement-based method also showed relatively good performance using yearly epochs. However, this method also led to false positive classifications of many non-glacier areas, such as the lake and the sloped terrain in the east and west. Low contrast areas are generally problematic for this method, leading to issues on water and snow surface, as outlined in existing research (Paul et al., 2017). Naturally, sloped, non-glaciated terrain is a constant error source for the presented method, as solifluction is a frequent process in this areas, which leads to surface displacements that are not connected to glacial activities (Pronk et al., 2021). Respective issues may be reduced by also introducing density-curve based thresholds and suitable filtering approaches (Kaufmann et al., 2019). Additionally, the result of the four-year period was characterized by many artefacts. Therefore, this method is only applicable with additional variables or rule-based approaches. Generally, there are numerous possibilities to substantially adapt and improve the presented method with field data, but such an approach is beyond a purely automatic method of debris-covered glacier demarcation. Finally, the presented methods are based on the assumption of glacier retreat and would have to be slightly adapted to also include glacier advances.

5. Conclusions

The presented test of different methods for automatically delineating debris-covered glaciers resulted in good performance, showing a difference of only 0.32 m to 0.97 m when compared to the geodetically derived glacial snout. Methods based on elevation differences also showed a good visual representation of the glacier area, with glaciated areas correctly identified as glaciers and no abundance of false positive mappings of non-glaciated surfaces, but the error assessment indicates that yearly surveys are a prerequisite for accurate demarcation. Displacement based methods showed lower performance, with errors between 0.51 m and 1.89 m, and a large number of wrongly assigned glacier areas, indicating that this method would benefit from further adjustments. In summary, this study provides an example for simple and automatic derivation of the glacier margin of debris-covered glaciers using high resolution UAV imagery. Derived error metrics show that the presented methodology allows accurate delineation of debris-covered glaciers and pro-glacial areas using an automated method, enabling increased standardization of remote sensing-based glacier monitoring.

Author contributions

Conceptualization: H.Z., W.S.; methodology: H.Z; software: H.Z.; formal analysis: H.Z.; investigation: H.Z., W.S.; resources and field work: H.Z., W.S., V.K.; data curation: H.Z., W.S., V.K.; writing – original draft preparation: H.Z.; writing – review and editing: H.Z., W.S., V.K.; visualization: H.Z.; supervision: W.S.

Data availability statement

Geodetic measurement data and selected photos are available at https://www.staff.tugraz.at/viktor.kaufmann/Goessnitzkees/index.html. UAV data may be obtained by contacting the corresponding author.

Acknowledgements

We thank the National Park Hohe Tauern for enabling scientific UAV surveys in the national park. We are also very grateful for the support of students from the Technical University of Graz and the University of Graz.

References

Aati, S., Milliner, C., and Avouac, J.-P. (2022). A new approach for 2-D and 3-D precise measurements of ground deformation from optimized registration and correlation of optical images and ICA-based filtering of image geometry artifacts. *Remote Sens. Environ.*, 277, 113038. DOI: 10.1016/j.rse.2022.113038.

Avian, M., Bauer, C., Schlögl, M. et al. (2020). The Status of Earth Observation Techniques in Monitoring High Mountain Environments at the Example of Pasterze Glacier, Austria: Data, Methods, Accuracies, Processes, and Scales. *Remote Sens.*, 12(8), 1251. DOI: 10.3390/rs12081251.

Azzoni, R.S., Fugazza, D., Zerboni, A. et al. (2018). Evaluating high-resolution remote sensing data for reconstructing the recent evolution of supra glacial debris: A study in the Central Alps (Stelvio Park, Italy). *Prog. Phys. Geogr. Earth Environ.*, 42(1), 3–23. DOI: 10.1177/0309133317749434.

Barr, I.D., Dokukin, M.D., Kougkoulos, I. et al. (2018). Using ArcticDEM to Analyse the Dimensions and Dynamics of Debris-Covered Glaciers in Kamchatka, Russia. *Geosci.*, 8(6), 216. DOI: 10.3390/geosciences8060216.

Bolch, T., Buchroithner, M. F., Kunert, A. et al. (2007). *Automated delineation of debris-covered glaciers based on ASTER data*. In M. A. Gomarasca (Ed.), GeoInformation in Europe, pp. 403–410. Netherlands: Millpress.

Borchers, H.W. (2023). pracma: Practical Numerical Math Functions. Retrieved November 10, 2024, from https://cran.r-project.org/web/packages/pracma/index.html. Accessed 4 September 2024.

Bremer. (2012). Module IMCORR – Feature Tracking / SAGA-GIS Module Library Documentation (v2.1.4). Retrieved September 4, 2024, from https://saga-gis.sourceforge.io/saga_tool_doc/2.1.4/grid_analysis_19.html.

Conrad, O., Bechtel, B., Bock, M. et al. (2015). System for Automated Geoscientific Analyses (SAGA) v. 2.1.4. *Geosci. Model Developemnt*, 8(7), 1991–2007. DOI: 10.5194/gmd-8-1991-2015.

Di Rita, M., Fugazza, D., Belloni, V. et al. (2020). Glacier volume change monitoring from UAV observations: issues and potentials of state-of-the-art techniques. *Int. Arch. Photogr. Remote Sens. Spatial Inf. Sci.*, XLIII-B2-2020, 1041–1048. DOI: 10.5194/isprs-archives-XLIII-B2-2020-1041-2020.

Ewertowski, M.W., Tomczyk, A.M., Evans, D.J.A. et al. (2019). Operational Framework for Rapid, Very-high Resolution Mapping of Glacial Geomorphology Using Low-cost Unmanned Aerial Vehicles and Structure-from-Motion Approach. *Remote Sens.*, 11(1), 65. DOI: 10.3390/rs11010065.

Fahnestock, M.A., Scambos, T.A., and Bindschadler, R.A. (1992). Semi-automated ice velocity determination from satellite imagery. *Eos*, 73(493), 437–461.

Fleischer, F., Otto, J., Junker, R. R., & Hölbling, D. (2021). Evolution of debris cover on glaciers of the Eastern Alps, Austria, between 1996 and 2015. Earth Surface Processes and Landforms, 46(9), 1673–1691. DOI: 10.1002/esp.5065.

Foster, L.A., Brock, B.W., Cutler, M.E J. et al. (2012). A physically based method for estimating supraglacial debris thickness from thermal band remote-sensing data. *J. Glaciol.,* 58(210), 677-691. DOI: 10.3189/2012JoG11J194.

Fugazza, D., Senese, A., Azzoni, R.S. et al. (2015). High-resolution mapping of glacier surface features. The UAV survey of the Forni glacier (Stelvio National Park, Italy). *Geografia Fisica e Dinamica Quaternaria*, 38, 25-33. DOI: 10.4461/GFDQ.2015.38.03.

Hijmans, R.J., Bivand, R., Dyba, K. et al. (2024). Terra: Spatial Data Analysis.Retrieved September 4, 2024, from https://cran.r-project.org/web/packages/terra/index.html.

Huss, M., and Fischer, M. (2016). Sensitivity of Very Small Glaciers in the Swiss Alps to Future Climate Change. *Fron. Earth Sci.*, 4. DOI: 10.3389/feart.2016.00034.

Immerzeel, W.W., Kraaijenbrink, P.D.A., Shea, J.M. et al. (2014). High-resolution monitoring of Himalayan glacier dynamics using unmanned aerial vehicles. *Remote Sens. Environ.*, 150, 93–103. DOI: 10.1016/j.rse.2014.04.025.

Jawak, S.D., Kumar, S., Luis, A.J. et al. (2018). Evaluation of Geospatial Tools for Generating Accurate Glacier Velocity Maps from Optical Remote Sensing Data. In The 2nd International Electronic Conference on *Remote Sensing*, p. 341. DOI: 10.3390/ecrs-2-05154.

Kaufmann, V., and Ladstädter, R. (2008a). Documentation of the Retreat of Gössnitzkees and Hornkees Glaciers (Hohe Tauern Range, Austria) for the Time Period 1997-2006 by Means of Aerial Photogrammetry. In Proceedings of the 6th ICA Mountain Cartography Workshop (Vol. 6, pp. 115–123). Lenk, Switzerland: Proceedings of the ICA Mountain Cartography Workshop. https://mountaincartography.icaci.org/publications/papers/papers_lenk_08/kaufmann.pdf.

Kaufmann, V., and Ladstädter, R. (2008b). Application of terrestrial photogrammetry for glacier monitoring in alpine environments. Proceedings of the 21st Congress of ISPRS, 37(Part B8), 813–818.

Kaufmann, V., and Sulzer, W. (2019). Dokumentation des Gletscherrückgangs am Gössnitzkees für den Zeitraum 1982-2018 – eine Gletschergeschichte mit Ablaufdatum.

Kaufmann, V., Sulzer, W., Seier, G. et al. (2019). Panta Rhei: Movement Change of Tschadinhorn Rock Glacier (Hohe Tauern Range, Austria). *Cartogr. Geoinf.,* 18(31), 4–24. DOI: 10.32909/kg.18.31.1.

Kaufmann, V. (2024). Website for access to geodetic measurement results of the Goessnitzkees (Carinthia, Austria). Retrieved October 18, 2024, from https://www.staff.tugraz.at/viktor.kaufmann/Goessnitzkees/index.html.

Kellerer-Pirklbauer, A. (2008). The Supraglacial Debris System at the Pasterze Glacier, Austria: Spatial Distribution, Characteristics and Transport of Debris. *Zeitschrift für Geomorphologie, Supplementary Issues*, 52(1), 3–25. DOI: 10.1127/0372-8854/2008/0052S1-0003.

Kellerer-Pirklbauer, A., Avian, M., Benn, D.I. et al. (2021). Buoyant calving and ice-contact lake evolution at Pasterze Glacier (Austria) in the period 1998–2019. The Cryosphere, 15(3), 1237–1258. *IEEE Access*, 8, 12725-12734. DOI: 10.5194/tc-15-1237-2021.

Khan, A.A., Jamil, A., Hussain, D. et al. (2020). Machine-Learning Algorithms for Mapping Debris-Covered Glaciers: The Hunza Basin Case Study. *IEEE Access*, 8, 12725–12734. DOI: 10.1109/ACCESS.2020.2965768.

Lambrecht, A., and Kuhn, M. (2007). Glacier changes in the Austrian Alps during the last three decades, derived from the new Austrian glacier inventory. *Ann. Glaciol.*, 46, 177–184. DOI: 10.3189/172756407782871341.

Land Kärnten. (1997). Orthophoto – Federal State of Kärnten – KAGIS. CC-BY-4.0. Retrieved March 20, 2024, from https://kagis.ktn.gv.at

Land Kärnten. (2012). Airborne Laserscanning Data – Federal State of Kärnten – KAGIS. CC-BY-4.0. Retrieved March 19, 2024, from https://kagis.ktn.gv.at.

Land Kärnten. (2021). Orthophoto – Federal State of Kärnten – KAGIS. CC-BY-4.0. Retrieved March 20, 2024, from https://kagis.ktn.gv.at.

Lang, H., and Lieb, G.K. (1993). Die Gletschere Kärntens. Klagenfurt, Austria: Verlag des Naturwissenschaftlichen Vereins für Kärnten.

Leprince, S., Barbot, S., Ayoub, F. et al. (2007). Automatic and Precise Orthorectification, Coregistration, and Subpixel Correlation of Satellite Images, Application to Ground Deformation Measurements. *IEEE Trans. Geosci. Remote Sens.*, 45(6), 1529–1558. DOI: 10.1109/TGRS.2006.888937.

Mayr, E., and Hagg, W. (2019). *Debris-Covered Glaciers*. In T. Heckmann & D. Morche (Eds.), Geomorphology of Proglacial Systems: Landform and Sediment Dynamics in Recently Deglaciated Alpine Landscapes, pp. 59–71. Cham: Springer International Publishing. DOI: 10.1007/978-3-319-94184-4_4.

Mölg, N., Bolch, T., Rastner, P. et al. (2018). A consistent glacier inventory for Karakoram and Pamir derived from Landsat data: distribution of debris cover and mapping challenges. *Earth Sys. Sci. Data*, 10(4), 1807–1827. DOI: 10.5194/essd-10-1807-2018.

Mueting, A., and Bookhagen, B. (2023). Tracking slow-moving landslides with PlanetScope data: new perspectives on the satellite's perspective (preprint). *EGUsphere [preprint]*. DOI: 10.5194/egusphere-2023-1698.

Patzelt, G. (1980). The Austrian glacier inventory: status and first results. Bremerhaven: IAHS Publication. Retrieved September 13, 2024, from https://epic.awi.de/id/eprint/32383/1/Patzelt_1980.pdf.

Paul, F., Huggel, C., and Kääb, A. (2004). Combining satellite multispectral image data and a digital elevation model for mapping debris-covered glaciers. *Remote Sens. Environ.*, 89(4), 510–518. DOI: 10.1016/j.rse.2003.11.007.

Paul, F., Bolch, T., Briggs, K. et al. (2017). Error sources and guidelines for quality assessment of glacier area, elevation change, and velocity products derived from satellite data in the Glaciers_cci project. *Remote Sens. Environ.*, 203, 256–275. DOI: 10.1016/j.rse.2017.08.038.

Pebesma, E. (2018). Simple Features for R: Standardized Support for Spatial Vector Data. *The R Journal*, 10(1), 439-446.

Pebesma, E., and Bivand, R. (2023). *Spatial Data Science: With Applications in R*. New York: Chapman and Hall/CRC. DOI: 10.1201/9780429459016.

Piermattei, L., Carturan, L., and Guarnieri, A. (2015). Use of terrestrial photogrammetry based on structure-from-motion for mass balance estimation of a small glacier in the Italian alps. *Earth Surf. Proc. Landforms*, 40(13), 1791–1802. DOI: 10.1002/esp.3756.

Pronk, J.B., Bolch, T., King, O. et al. (2021). Contrasting surface velocities between lake- and land-terminating glaciers in the Himalayan region. *The Cryosphere*, 15(12), 5577–5599. DOI: 10.5194/tc-15-5577-2021.

R Core Team. (2024). R: A Language and Environment for Statistical Computing. Vienna, Austria: R Foundation for Statistical Computing. https://www.R-project.org/.

Robson, B.A., Hölbling, D., Nuth, C. et al. (2016). Decadal Scale Changes in Glacier Area in the Hohe Tauern National Park (Austria) Determined by Object-Based Image Analysis. *Remote Sens.*, 8(1), 67. DOI: 10.3390/rs8010067.

Sahu, R., and Gupta, R.D. (2018). Conceptual framework of the combined pixel and object-based method for the delineation of debris-covered glaciers. *ISPRS Ann. Photogr. Remote Sens. Spatial Inf. Sci.*, IV–5, 173–180. DOI: 10.5194/isprs-annals-IV-5-173-2018.

Scambos, T.A., Dutkiewicz, M.J., Wilson, J.C. et al. (1992). Application of image cross-correlation to the measurement of glacier velocity using satellite image data. *Remote Sens. Environ.*, 42(3), 177–186. DOI: 10.1016/0034-4257(92)90101-O.

Shukla, A., and Garg, P. K. (2019). Evolution of a debris-covered glacier in the western Himalaya during the last four decades (1971–2016): A multiparametric assessment using remote sensing and field observations. *Geomorphology*, 341, 1–14. DOI: 10.1016/j.geomorph.2019.05.009.

Sledz, S., Ewertowski, M.W., and Piekarczyk, J. (2021). Applications of unmanned aerial vehicle (UAV) surveys and Structure from Motion photogrammetry in glacial and periglacial geomorphology. *Geomorphology*, 378, 107620. DOI: 10.1016/j.geomorph.2021.107620.

Strimas-Mackey, M. (2023). smoothr: Smooth and Tidy Spatial Features. Retrieved September 4, 2024, from https://cran.r-project.org/web/packages/smoothr/index.html.

Thomas, D. J., Robson, B. A., & Racoviteanu, A. (2023). An integrated deep learning and object-based image analysis approach for mapping debris-covered glaciers. Frontiers in Remote Sensing, 4, 1161530. DOI: 10.3389/frsen.2023.1161530.

Tielidze, L.G., Iacob, G., and Holobâcă, I.H. (2024). Mapping of Supra-Glacial Debris Cover in the Greater Caucasus: A Semi-Automated Multi-Sensor Approach. *Geosci.*, 14(7), 178. DOI: 10.3390/geosciences14070178.

Wecht, M. (2021). Standardized structure from motion – multi view stereo photogrammetry workflow to gain high quality digital elevation models for geomorphic research. Master Thesis TU Graz. DOI: 10.3217/2s19x-n9x81.

Westoby, M.J., Brasington, J., Glasser, N.F. et al. (2012). 'Structure-from-Motion' photogrammetry: A low-cost, effective tool for geoscience applications. *Geomorphology*, 179, 300–314. DOI: 10.1016/j.geomorph.2012.08.021.

Xie, Z., Haritashya, U.K., Asari, V.K. et al. (2020). GlacierNet: A Deep-Learning Approach for Debris-Covered Glacier Mapping. *IEEE Access*, 8, 83495–83510. DOI: 10.1109/ACCESS.2020.2991187.

Yang, X., Xie, F., Liu, S. et al. (2024). Mapping Debris-Covered Glaciers Using High-Resolution Imagery (GF-2) and Deep Learning Algorithms. *Remote Sens.*, 16(12), 2062. DOI: 10.3390/rs16122062.

Yurtseven, H. (2019). Comparison of GNSS-, TLS- and Different Altitude UAV-Generated Datasets on the Basis of Spatial Differences. *ISPRS Int. J. Geo-Inf.*, 8(4), 175. DOI: 10.3390/ijgi8040175.

Zandler, H., Haag, I., and Samimi, C. (2019). Evaluation needs and temporal performance differences of gridded precipitation products in peripheral mountain regions. *Sci. Rep.*, 9(1), 15118. DOI: 10.1038/s41598-019-51666-z.

Zhou, W., Xu, M., and Han, H. (2024). Spatial Distribution and Variation in Debris Cover and Flow Velocities of Glaciers during 1989–2022 in Tomur Peak Region, Tianshan Mountains. *Remote Sens.*, 16(14), 2587. DOI: 10.3390/rs16142587.